

Orbital magnetic field driven metal-insulator transition in strongly correlated electron systems

Georg Rohringer^{1,2} and Anton Markov^{3,4}

¹*Institute of Theoretical Physics, University of Hamburg, 20355 Hamburg, Germany*

²*Theory and Simulation of Condensed Matter, Department of Physics, King's College London, The Strand, London WC2R 2LS, United Kingdom*

³*Russian Quantum Center, Skolkovo Innovation City, 121205 Moscow, Russia*

⁴*Department of Physics, Lomonosov Moscow State University, Leninskie gory 1, 119991 Moscow, Russia*

We study the Mott metal-insulator transition in the Hubbard-Hofstadter model as a function of the orbital magnetic field, exploiting dynamical mean field theory (DMFT). Considering interaction strengths between the electrons for which this model is in the Mott insulating state in the field-free case, we find that for sufficiently large magnetic fields a metallic phase emerges. Upon decreasing the field, we observe a metal-insulator transition from this metallic to an insulating state. This effect can be understood by a magnetic field induced increase of the kinetic energy due to the formation of magnetic mini-bands which enhances the ratio between the kinetic and potential energy and can, thus, trigger a transition between a metallic and insulating phase. Our findings are in good qualitative agreement with a recent experiment [Nature Communications 11, 3591] on vanadium oxide (VO₂) where a magnetic field driven insulator-to-metal transition has been observed at strong magnetic fields.

PACS numbers: 71.27.+a 71.10.Fd

Introduction. Transitions between metallic and insulating states in solids play a fundamental role in condensed matter physics. Apart from their theoretical importance they are potentially also technologically highly relevant as they can serve as switches to control electrical current. There exists a variety of distinct types of insulators which are driven by very different physical mechanisms: Band insulators[1] emerge due to the absence of spectral weight at the Fermi level, Slater insulators are induced by strong (antiferromagnetic) spin fluctuations[2], in Anderson insulators[3, 4] disorder leads to a localization of particles, Peierl's insulators[5] originate from structural changes of the underlying lattice system, and in charge transfer insulators[6] electrons or holes are transferred from the conduction to the valence band by correlation effects. A particularly interesting class are Mott insulators[7] where the insulating state is induced by correlation effects between their electrons due to the strong Coulomb repulsion. Typical examples for Mott insulators are transition metal dichalcogenides[8, 9] such as 1T-TaS₂ or 1T-TaSe₂[10], Nickelates such as RNiO₃[11] or transition metal oxides[12, 13] such as V₂O₃[14–16].

The transition between the metallic and the Mott insulating state can be triggered by different control parameters including temperature, strain[17], doping[18], (chemical) pressure, or even electric fields[19]. Importantly for the context of this work, the transition between a metal and an insulator can be also controlled by the application of an external magnetic field[20, 21]. A good example for such a phenomenon in strongly correlated electron systems is the colossal magneto resistance observed in Manganites[22–24] where an external magnetic field can change the resistivity by several orders of

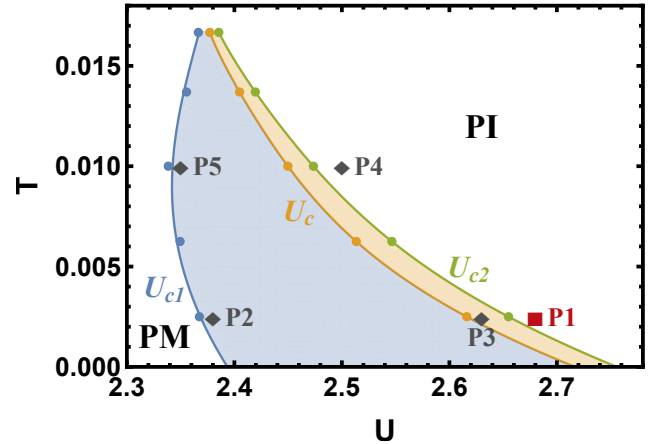


FIG. 1. DMFT phase diagram of the 2d Hubbard model on a simple (bipartite) square lattice as a function of interaction strength U and temperature T at magnetic field $B = 0$. U_{c1} and U_{c2} are the boundaries between the coexistence region and the paramagnetic metallic (PM) and paramagnetic insulating (PI) phase, respectively, while U_c corresponds to the line where the thermodynamic phase transition occurs. P1 to P5 indicate the points for which calculations at finite orbital magnetic fields have been performed.

magnitude.

Recently, also the response of the prototypical strongly correlated transition metal oxide VO₂ to very large magnetic fields has been investigated[25, 26]. In these experiments, a transition from an insulator at zero field to a metal at a magnetic field of about 500T was observed. It has been proposed, that the change in conductivity

is triggered by the impact of the magnetic field on the spins of the Vanadium d electrons (i.e., the spin Zeeman effect). However, as the authors argue themselves, this effect might not be sufficient to explain the observed experimental results comprehensively as the energy scale of the Zeeman term is substantially smaller than the band splitting in the insulating phase. This has motivated us to study the *orbital effects* of a magnetic field in a strongly correlated electron system which have been addressed so far only sporadically[27–32]. To this end, we consider the single-band Hubbard-Hofstadter model where a magnetic field is coupled to the orbital degrees of freedom by introducing a Peierl’s phase in the hopping parameter. We investigate this model exploiting the recently developed extension of dynamical mean field theory (DMFT)[33–36] to finite magnetic fields[28–31]. Our analysis of the free energy, double occupancy and (inverse) quasi-particle lifetime predicts the emergence of a metallic state inside the Mott insulating phase of the field-free system for sufficiently large magnetic fields and a transition to the insulating state upon decreasing the magnetic field. The field strength at which the transition occurs in our theoretical calculations is in good qualitative agreement with experimental findings for VO₂ in Ref. [25, 26] and might also contribute to the understanding of recent corresponding results for λ -type organic conductors[37].

Model and Method. We consider the (bipartite) single-band half filled Hubbard model on a simple square lattice with a hopping amplitude t between neighboring sites for different interaction strengths U within or close to the coexistence region between the metallic and the insulating states at selected temperatures T . The orbital magnetic field is introduced by adding a Peierl’s phase to the hopping term[28, 29, 38]. We consider magnetic field strengths $B = \frac{p}{q} \frac{\Phi_0}{a^2}$ where $\Phi_0 = \frac{h}{e}$ is the flux quantum, a is the lattice constant and $p, q \in \mathbb{N}$ are coprime positive integers with $2p \leq q$ allowing for the definition of a commensurate magnetic unit cell of size q . DMFT is exploited to calculate the (local) self-energy as well as the kinetic, potential and free energies of the system. The associated impurity problem has been solved with exact diagonalization (ED) and carefully benchmarked for selected parameters against a continuous time quantum Monte Carlo (CTQMC) algorithm[39] (see Sec. S4 in the supplemental material(SM)[38]). More technical details are provided in Sec. S1 of the SM[38]. In the following, we will use the half bandwidth $\frac{W}{2} = 4t$ at $B = 0$ as unit of energy while the magnetic field is expressed in terms of $\frac{\Phi_0}{a^2}$ (i.e., by the dimensionless quantity $B \sim \frac{p}{q}$). For convenience we set $\hbar = k_B = 1$ allowing us to express temperature and inverse time in terms of our energy unit $\frac{W}{2}$.

Results. Fig. 1 shows the phase diagram of the 2d half filled Hubbard model at $B = 0$ as a function of interaction strength U and temperature T . The blue and green

lines indicate the borders U_{c1} and U_{c2} of the coexistence region where both the insulating and the metallic state of the system can be stabilized in DMFT. On the left of U_{c1} and on the right of U_{c2} the system is a paramagnetic metal (PM) and a paramagnetic insulator (PI), respectively. In the blue shaded part of the coexistence area the metallic solution features the lower free energy while in the orange shaded region the lower free energy is obtained for the insulating state. At the orange line both free energies coincide which marks the thermodynamic first-order phase transition between the two regimes. Calculations at finite magnetic fields have been performed for the parameters indicated by the points P1 to P5. The results for P1 (red square) are presented in the paper while the data for P2 to P5 (grey diamonds) are provided in the SM[38].

Figure 2 shows the results for the point P1 in the phase diagram of Fig. 1, corresponding to the interaction strength $U = 2.68$ and the temperature $T = 0.0025$ where the system is a Mott insulator for $B = 0$. In the left panel, the free energy F is depicted as a function of the magnetic field B for two different sets of calculations indicated by B_{\uparrow} and B_{\downarrow} . For the first set B_{\uparrow} , we started from the (insulating) state S1 at $B = 0$ and gradually increased the magnetic field (dashed purple line). The free energy evolves smoothly and no sign of a (first order) phase transition is observed, i.e., the system remains in its initial thermodynamic state. For the second set of calculations B_{\downarrow} , we started at $B = 0.5$ and gradually decreased the magnetic field (green solid line). Remarkably, at $B = 0.5$ we can stabilize not only the state S1 but our DMFT equations feature a second solution S2 with a substantially lower free energy. Upon decreasing B the difference in the free energy between the two solutions diminishes and eventually vanishes at a critical field strength $B_c = 0.2077$, indicating a thermodynamic phase transition from S2 to S1. Nevertheless, we can stabilize S2 for even smaller values of the magnetic field $B < B_c$, where its free energy is already larger than the one of S1, until the phase S2 gets unstable at $B_{c2} = 0.1259$ and collapses onto S1. This behavior is indicative for a first order phase transition where B_{c2} marks the border of the coexistence region of states S1 and S2. Let us note, that the other border B_{c1} after which the system is always in state S2, has not been reached for the largest magnetic field $B = 0.5$ [40] (see Sec. S2 of the SM[38]).

To analyze the physical nature of the two solutions S1 and S2 in more detail we have calculated the double occupancy $D = \langle n_{\uparrow} n_{\downarrow} \rangle$ as a function of the magnetic field B which is shown in the middle panel of Fig. 2. For solution S1 (empty purple squares), the double occupancy is very small over the entire B range indicating that the system remains in the insulating state from which it started at $B = 0$. On the contrary, solution S2 (green filled circles) features substantially larger values of D for magnetic fields $B > B_{c2}$, indicative of a metallic state of the

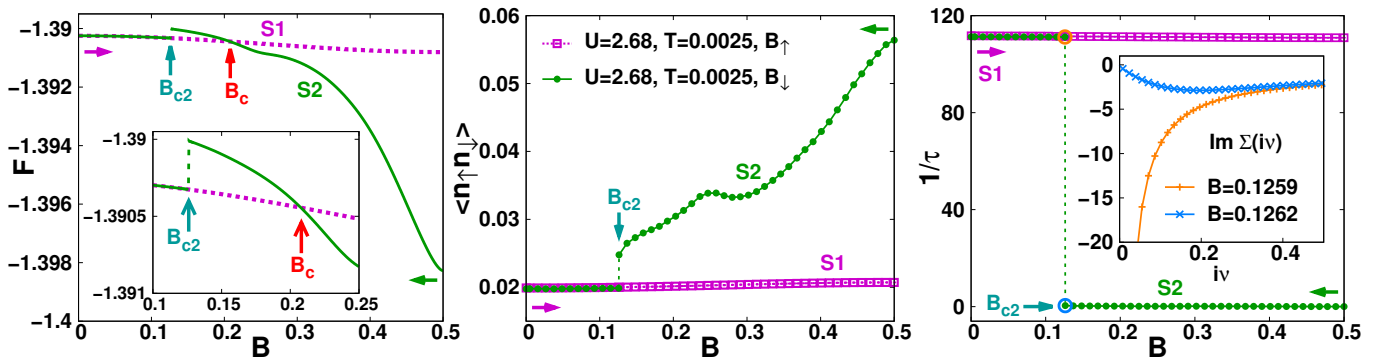


FIG. 2. Free energy F (left panel), double occupancy $D = \langle n_{\uparrow} n_{\downarrow} \rangle$ (middle panel) and inverse quasiparticle lifetime $1/\tau$ (right panel) for the parameter set P1 in Fig. 1 corresponding to $U=2.68$ and $T=0.0025$, as a function of the orbital magnetic field B . The inset in the left panel is a blow up of the transition region. The Inset in the right panel shows the electronic self-energy $\Sigma(i\nu)$ as a function of Matsubara frequency for magnetic fields right before and right after the point B_{c2} where the metallic solution becomes unstable (marked by blue and orange circles in the main panel). B_{\uparrow} and B_{\downarrow} indicate that calculations have bin started from $B=0$ or $B=0.5$, respectively.

Hubbard-Hofstadter model in this parameter regime. As for the free energy in the left panel, both curves become equivalent for $B < B_{c2}$ where the insulating state is the only solution of our DMFT equations.

The above scenario of a magnetic-field-driven metal-to-insulator transition is also confirmed by the analysis of the inverse quasiparticle lifetime $1/\tau$ in the right panel of Fig. 2. At small temperatures this quantity can be (approximately) obtained from the local frequency dependent DMFT self-energy $\Sigma(i\nu)$ on the imaginary (Matsubara) frequency axis: $1/\tau \sim -\text{Im}\Sigma(i\nu_1)$ at the first Matsubara frequency $\nu_1 = \frac{\pi}{\beta}$. A small value of this observable corresponds to a long lifetime of well-defined single particle excitation typically observed in the metallic state of correlated electron systems. A large value of $1/\tau$ on the other hand indicates the absence of coherent quasiparticles which is a hallmark of the Mott insulating phase. For the state S1 (empty purple squares) we indeed find such a large value of $1/\tau$ at all magnetic fields confirming the Mott insulating nature of this solution of our DMFT equations. On the contrary, for S2 (green filled circles) the inverse quasiparticle life time is small at $B=0.5$ and only slightly increases upon decreasing the magnetic field as long as $B \geq B_{c2}$. Hence, the system is a metal within this range of magnetic fields. At $B=B_{c2}$ the inverse life time features a discontinuity confirming the transition to the insulating state at this magnetic field.

The rapid change of state for solution S2 at B_{c2} is also clearly visible in the imaginary part of the self-energy $\text{Im}\Sigma(i\nu)$ as a function of Matsubara frequency in the inset of the right panel of Fig. 2. For the magnetic field $B=0.1262$ slightly above the transition (blue crosses) we observe a non-monotonous behavior at low frequencies with an upturn of $\text{Im}\Sigma(i\nu)$ upon approaching $\nu=0$ which is typical for a metallic (Fermi liquid like) self-energy. On the contrary, for the slightly smaller magnetic field $B=0.1259$ (orange pluses) we find a monotonous

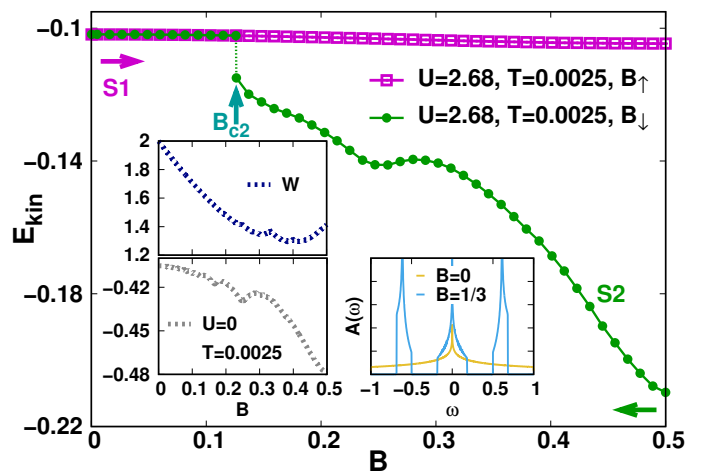


FIG. 3. Kinetic Energy for $U=2.68$ and $T=0.0025$ (point P1 in Fig. 1) as a function of the orbital magnetic field B obtained by the two sets of calculations B_{\uparrow} and B_{\downarrow} discussed in Fig. 2. Left upper inset: Bandwidth W of the non-interacting system as a function of the magnetic field; Left lower inset: Kinetic energy for $U=0$ and $T=0.0025$; Right lower inset: Non-interacting density of states as a function of single-particle energy ω for $B=0$ and $B=\frac{1}{3}$.

behavior with a diverging self-energy for $\nu \rightarrow 0$ indicative of a Mott insulator.

Discussion. Let us now address the question which physical mechanism is at work to drive the transition between a metal and an insulator upon tuning the magnetic field B . We start by investigating how this orbital magnetic field modifies the bandwidth W of the system. In the left upper inset of Fig. 3 we observe that W is *reduced* when B increases. From this behavior we would, however, naively expect that for a fixed interaction strength the system becomes more insulating rather than more metallic at larger orbital magnetic

fields. Hence, since the change in the bandwidth cannot explain the observed phase transition, we have turned our attention to the behavior of the kinetic energy as a function of B . This thermodynamic observable is indeed *enhanced* (in absolute value) upon increasing B as it can be seen already for the non-interacting case in the left lower inset of Fig. 3. Such an increase of E_{kin} with increasing magnetic field also persists when we switch on the interactions (main panel of Fig. 3). As expected, E_{kin} is larger and changes more rapidly for the metallic solution S2 (green filled circles) when $B > B_{c2}$ compared to the insulating state (empty purple squares and green filled circles for $B < B_{c2}$). The increase of kinetic energy with B might be explained by a shift of spectral weight from the Fermi energy $\epsilon_F = 0$ to the magnetic subbands at higher energies (right inset of Fig. 3). The van Hove singularity at $\omega \approx -0.55$ for $B = \frac{1}{3}$ gives indeed rise to a large contribution to E_{kin} while the van Hove singularity at $\omega = -$ for $B = 0$ is almost irrelevant for the value of this thermodynamic observable.

We can interpret the enhancement of the kinetic energy by the orbital magnetic field as a metallization effect which reduces the impact of the Hubbard interaction U . Such a suppression of correlations by B has indeed already been observed in a recent determinant quantum Monte Carlo (DQMC) study[32] where also the increase of the kinetic energy with increasing field has been reported. Moreover, a corresponding reduction of the Mott gap for larger values of B has been found in an ED study of a finite system[27]. However, to the best of our knowledge, it has not been demonstrated so far, that this metallization effect of the orbital magnetic field is strong enough to actually drive the Mott transition without any accompanying modification of the interaction strength U .

Relation to experimental studies. In a recent experiment[25, 26] a magnetic field driven transition from an insulating to a metallic state has been found in Tungsten-doped Vanadium oxide $V_{1-x}W_xO_2$ at doping $x = 0.06$, and $B = 500\text{T}$. Let us note, that for the corresponding metal-insulator transition in this material at $B = 0$ there is an intense and still ongoing debate whether correlation effects (Mott transition) or a change in the lattice structure (Peierl's transition) are responsible for the emergence of the insulating state. In the latter scenario, the insulator originates from the formation of V-V dimers which are stabilized by electrons with opposite spin in the d -orbitals of the two V atoms. Within this picture, an applied magnetic field aligns the spins of the electrons in the molecular orbital leading to the dissociation of the dimer and, consequently, a reappearance of the metallic state. However, as the authors themselves point out in their paper, the Zeeman energy of the spin 1/2 electrons $E_Z \sim 0.058\text{eV}$ (for $B = 500\text{T}$) is two orders of magnitude smaller than the energy separation between the bonding and the antibonding state of

the dimer $\Delta E_{\text{Dimer}} \sim 2.5\text{eV}$. Hence, they conclude that the observed insulator-to-metal transition cannot solely be explained by the impact of the magnetic field on the spins and correlation effects should play an important role.

Our numerical analysis suggests that a more comprehensive understanding of the problem can be achieved by taking into account the orbital effects of the magnetic field for the observed phase transition. To compare our results to the experimental findings we estimate the critical temperature where the phase transition occurs in our phase diagram in Fig. 1 as $T_c \sim 0.0166$. The temperature ratio $\frac{T}{T_c} \sim 0.15$ for our calculations in Fig. 2 is then close to the corresponding value 0.14 for which the experiments on VO_2 have been conducted in Ref. [25]. Considering a lattice constant $a = 6\text{\AA}$ which is compatible with both experimental findings and theoretical predictions[41] our numerical results correspond to a phase transition at $B_{\text{crit}} = B_c \frac{\Phi_0}{a^2} \sim 1200\text{T}$. Although this is larger than the experimental value of $B_{\text{exp}} = 500$ by a factor of two it is of the same order of magnitude and, hence, in qualitative agreement with the experimental figure. In this respect, let us note that a better quantitative agreement for the critical magnetic field could be easily achieved by slightly reducing the interaction parameter U as the system will become more metallic, resulting in a smaller B_c compared to the one obtained in Fig. 2. Such a lower critical field emerges for $U = 2.63$ and $T = 0.0025$ (point P3 in the phase diagram of Fig. 1) in Fig. S3 of Sec. S3 of the SM[38] for which $B_c = 0.0946$ corresponding to $B_{\text{crit}} \sim 540\text{T}$ is found. In fact, an exact reproduction of the experimental figures would require a realistic estimation of the interaction parameter in VO_2 which is, however, not in the scope of this paper. Instead, our aim is to demonstrate the possibility of an orbital magnetic field driven metal-insulator transition and its compatibility with experimental results.

Our theoretical analysis can also explain why no metal-insulator transition has been observed in the experiment for lower W-doping in the considered range of the magnetic field. In our calculations, the magnitude of the magnetic flux through a unit cell rather than the magnetic field itself is the decisive quantity for the emergence of the phase transition. Hence, since the lattice constant in $V_{1-x}W_xO_2$ decreases with decreasing doping[42] a gradually increasing magnetic field is required to generate the same total flux through a unit cell at which the phase transition is observed.

The discussion above suggests, that correlation effects play a crucial role for the experimentally observed metal-insulator transition in W-doped VO_2 . Hence, our theoretical study supports the Mott scenario for this transition which is also indicated by a recent broadband optical spectroscopy experiments[43]. Let us, however, note that within our single-band analysis we cannot address the impact of the orbital magnetic field on the dimer formation

which might support the dissociation of the V dimers in a Peierl's-like transition. This interesting question requires a modelling of the problem beyond the simple sing-band Hubbard-Hofstadter Hamiltonian (including the Zeeman term) which represents an interesting future research perspective.

Let us briefly mention a second experimental study where a magnetic field driven metal-insulator transition has been recently observed in λ -type organic conductors[37] at around $B \sim 50\text{T}$ whereas our study would predict $B \sim 290\text{T}$ due to the large size of the unit cell ($a \sim 12\text{\AA}$). It should be, however, noted that these materials feature a highly complicated molecular structure and further theoretical investigations beyond a simple single-band description might be required to obtain a comprehensive understanding of the role of orbital effects of the magnetic field for the metal-insulator transition in these compounds.

Conclusions and Outlook. We have demonstrated the emergence of a metal-insulator transition in the Hubbard-Hofstadter model which is driven by the orbital effect of an external magnetic field on the electrons. As for the more standard interaction driven MIT we observe a first order behavior with a coexistence region extending to a magnetic field B_{c2} while the actual thermodynamic transition occurs at $B_c > B_{c2}$. We have argued that this magnetic-field-driven change of state can be explained by a metallization effect due to the orbital magnetic field which is indicated by the increase of the kinetic energy with increasing B . In the final part of the paper, we have discussed the relevance of our results for recent experiments on VO_2 and λ -type organic conductors and argue that orbital effects of an external magnetic field might play an important role for the magnetic field induced metal-insulator transition in these materials.

In general, the importance of the orbital effects of a magnetic field with respect to the spin Zeeman term can be investigated experimentally by changing the size of the unit cell (e.g., by pressure or doping). While such a change in the lattice structure should affect the Zeeman splitting only linearly it enters quadratically in the orbital magnetic field. Another possibility to disentangle the spin and orbital effects of magnetic fields are synthetic gauge fields generated by lasers with periodic driving which couple only to orbital degrees of freedom. On the theoretical side, we plan to extend our DMFT calculations to a larger set of interaction parameters, temperatures and lattice types to map out a comprehensive phase diagram for the orbital-magnetic-field-driven metal-insulator transition in correlated electron systems.

Acknowledgements. We thank T. Schäfer, A. Toschi and G. Sangiovanni for useful discussions. G. R. acknowledges financial support from the Deutsche Forschungsgemeinschaft (DFG) through Projects No. 407372336 and No. 449872909. A. A. M acknowledges support from the Russian Quantum Center in the framework of the

Russian Quantum Technologies Roadmap. The authors gratefully acknowledge the computing time granted by the Resource Allocation Board and provided on the supercomputers Lise and Emmy/Grete at NHR@ZIB and NHR@Göttingen as part of the NHR infrastructure. The calculations for this research were conducted with computing resources under the project hhp00048.

-
- [1] N. Ashcroft and N. Mermin, *Solid State Physics* (Harcourt College Publishers, New York, 1976).
 - [2] T. Schäfer, F. Geles, D. Rost, G. Rohringer, E. Arrigoni, K. Held, N. Blümer, M. Aichhorn, and A. Toschi, *Phys. Rev. B* **91**, 125109 (2015).
 - [3] P. W. Anderson, *Phys. Rev.* **109**, 1492 (1958).
 - [4] F. Evers and A. D. Mirlin, *Rev. Mod. Phys.* **80**, 1355 (2008).
 - [5] R. E. Peierls, *Quantum theory of solids* (Clarendon Press, 1996).
 - [6] J. Zaanen, G. A. Sawatzky, and J. W. Allen, *Phys. Rev. Lett.* **55**, 418 (1985).
 - [7] N. F. Mott, *Rev. Mod. Phys.* **40**, 677 (1968).
 - [8] S. Manzeli, D. Ovchinnikov, D. Pasquier, O. V. Yazyev, and A. Kis, *Nature Reviews Materials* **2**, 17033 (2017).
 - [9] B. H. Moon, *Emergent Materials* **4**, 989 (2021).
 - [10] Y. Fei, Z. Wu, W. Zhang, and Y. Yin, *AAPPS Bulletin* **32**, 20 (2022).
 - [11] K. Haule and G. L. Pascut, *Scientific Reports* **7**, 10375 (2017).
 - [12] K. Held, *Advances in Physics* **56**, 829 (2007).
 - [13] M. Imada, A. Fujimori, and Y. Tokura, *Rev. Mod. Phys.* **70**, 1039 (1998).
 - [14] D. B. McWhan, T. M. Rice, and J. P. Remeika, *Phys. Rev. Lett.* **23**, 1384 (1969).
 - [15] D. B. McWhan and J. P. Remeika, *Phys. Rev. B* **2**, 3734 (1970).
 - [16] McWhan, D. B., Menth, A., Remeika, J. P., Brinkman, W. F., and T. M. Rice, *Phys. Rev. B* **7**, 1920 (1973).
 - [17] K. L. Gurunatha, S. Sathasivam, J. Li, M. Portnoi, I. P. Parkin, and P. I., *Adv. Funct. Mater.* **30**, 2005311 (2020).
 - [18] C. Ling, Z. Zhao, X. Hu, J. Li, X. Zhao, Z. Wang, Y. Zhao, and H. Jin, *ACS Appl. Nano Mater.* **2**, 6738 (2019).
 - [19] G. Mazza, A. Amaricci, M. Capone, and M. Fabrizio, *Phys. Rev. Lett.* **117**, 176401 (2016).
 - [20] F. Kagawa, T. Itou, K. Miyagawa, and K. Kanoda, *Phys. Rev. Lett.* **93**, 127001 (2004).
 - [21] Z. L. Sun, A. F. Wang, H. M. Mu, H. H. Wang, Z. F. Wang, T. Wu, Z. Y. Wang, X. Y. Zhou, and X. H. Chen, *npj Quantum Materials* **6**, 94 (2021).
 - [22] A. P. Ramirez, *Journal of Physics: Condensed Matter* **9**, 8171 (1997).
 - [23] E. Dagotto, T. Hotta, and A. Moreo, *Physics Reports* **344**, 1 (2001).
 - [24] M. B. Salamon and M. Jaime, *Rev. Mod. Phys.* **73**, 583 (2001).
 - [25] Y. H. Matsuda, D. Nakamura, A. Ikeda, S. Takeyama, Y. Suga, H. Nakahara, and Y. Muraoka, *Nature Communications* **11**, 3591 (2020).
 - [26] Y. H. Matsuda, Y. Muraoka, D. Nakamura, A. Ikeda,

- Y. Ishii, X.-G. Zhou, H. Sawabe, and S. Takeyama, *Journal of the Physical Society of Japan* **91**, 101008 (2022), <https://doi.org/10.7566/JPSJ.91.101008>.
- [27] K. Czajka, A. Gorczyca, M. M. Maška, and M. Mierzejewski, *Phys. Rev. B* **74**, 125116 (2006).
- [28] S. Acheche, L.-F. Arsenault, and A.-M. S. Tremblay, *Phys. Rev. B* **96**, 235135 (2017).
- [29] A. A. Markov, G. Rohringer, and A. N. Rubtsov, *Phys. Rev. B* **100**, 115102 (2019).
- [30] J. c. v. Vučičević and R. Žitko, *Phys. Rev. Lett.* **127**, 196601 (2021).
- [31] J. Vučičević and R. Žitko, *Phys. Rev. B* **104**, 205101 (2021).
- [32] J. K. Ding, W. O. Wang, B. Moritz, Y. Schattner, E. W. Huang, and T. P. Devereaux, *Communications Physics* **5**, 204 (2022).
- [33] D. Vollhardt and P. Wölfe, “Electronic phase transitions,” (Elsevier Science Publishers B.V., 1992) Chap. 1, pp. 1–78.
- [34] A. Georges and W. Krauth, *Phys. Rev. Lett.* **69**, 1240 (1992).
- [35] A. Georges and G. Kotliar, *Phys. Rev. B* **45**, 6479 (1992).
- [36] A. Georges, G. Kotliar, W. Krauth, and M. J. Rozenberg, *Rev. Mod. Phys.* **68**, 13 (1996).
- [37] S. Fukuoka, T. Oka, Y. Ihara, A. Kawamoto, S. Imajo, and K. Kindo, *Phys. Rev. B* **109**, 195142 (2024).
- [38] G. Rohringer and A. Markov, “Magnetic field driven metal-insulator transition in strongly correlated electron systems,” (2024).
- [39] M. Wallerberger, A. Hausoel, P. Gunacker, A. Kowalski, N. Parragh, F. Goth, K. Held, and G. Sangiovanni, *Computer Physics Communications* **235**, 388 (2019).
- [40] Larger magnetic fields ($B > 0.5$) are not meaningful in our model since it is symmetric under the transformation $\frac{p}{q} \rightarrow 1 - \frac{p}{q}$.
- [41] Reported values for the hopping parameters of VO₂ and V_{1-x}W_xO₂ range from $a = 5.5\text{\AA}$ to $a = 9.0\text{\AA}$ in theoretical[44] and experimental[42] studies depending on the structural phase of the compound, the substrate on which it is grown as thin film and the amount of Tungsten doping. We have selected an intermediate value as we are not aiming at a precise quantitative reproduction but rather a qualitative understanding and an explanation of the order of magnitude of the experimental figures.
- [42] S. Choi, G. Ahn, S. J. Moon, and S. Lee, *Scientific Reports* **10**, 9721 (2020).
- [43] T. J. Huffman, C. Hendriks, E. J. Walter, J. Yoon, H. Ju, R. Smith, G. L. Carr, H. Krakauer, and M. M. Qazilbash, *Phys. Rev. B* **95**, 075125 (2017).
- [44] H. Lu and J. Robertson, *physica status solidi (b)* **256**, 1900210 (2019), <https://onlinelibrary.wiley.com/doi/pdf/10.1002/pssb.201900210>.

Orbital magnetic field driven metal-insulator transition in strongly correlated electron systems — Supplemental Material

Georg Rohringer^{1,2} and Anton Markov^{3,4}

¹*Institute of Theoretical Physics, University of Hamburg, 20355 Hamburg, Germany*

²*Theory and Simulation of Condensed Matter, Department of Physics, King's College London, The Strand, London WC2R 2LS, United Kingdom*

³*Russian Quantum Center, Skolkovo Innovation City, 121205 Moscow, Russia*

⁴*Department of Physics, Lomonosov Moscow State University, Leninskie gory 1, 119991 Moscow, Russia*

PACS numbers: 71.27.+a 71.10.Fd

S1. CALCULATION OF THE FREE ENERGY WITHIN DMFT

In this section, we provide a number of technical details for our DMFT calculations. More specifically, in Sec. S1A we discuss the Hubbard-Hofstadter Hamiltonian and the DMFT approach to treat it. In Sec. S1B we present the calculation of the free energy and in Sec. S1C we outline specific numerical improvements which has allowed us to perform calculations on a very fine B grid.

A. DMFT for the Hubbard-Hofstadter model

The Hamiltonian of the Hubbard-Hofstadter model is given by

$$\hat{H} = -t \sum_{\langle ij \rangle, \sigma} f_{ij} \hat{c}_{i\sigma}^\dagger \hat{c}_{j\sigma} + U \sum_i \hat{n}_{i\uparrow} \hat{n}_{i\downarrow}, \quad (\text{S.1})$$

where $\hat{c}_{i\sigma}^{(\dagger)}$ annihilates (creates) an electron with spin $\sigma = \uparrow, \downarrow$ at lattice site \mathbf{R}_i , $\hat{n}_{i\sigma} = \hat{c}_{i\sigma}^\dagger \hat{c}_{i\sigma}$ denotes the number of particles at lattice site \mathbf{R}_i , t is the hopping amplitude between two neighboring sites \mathbf{R}_i and \mathbf{R}_j of the simple square lattice and U corresponds the local Coulomb interaction between two particles at the same lattice site \mathbf{R}_i . The magnetic field dependence is encoded in the

Peierl's phase factor

$$f_{ij} = \exp \left\{ i \frac{2\pi}{\Phi_0} \int_{\mathbf{R}_i}^{\mathbf{R}_j} \mathbf{A}(\mathbf{r}) \cdot d\mathbf{r} \right\}. \quad (\text{S.2})$$

The vector potential $\mathbf{A}(\mathbf{r})$ for the uniform magnetic field in z -direction $\mathbf{B} = (0, 0, B)$ in the Landau gauge is given by

$$\mathbf{A}(\mathbf{r}) = -B \begin{pmatrix} y \\ 0 \\ 0 \end{pmatrix}. \quad (\text{S.3})$$

This formally breaks translational invariance of the system in y -direction, although from a physical perspective the system should remain homogeneous for a constant magnetic field. However, for magnetic fields which are rational multiples of the flux quantum Φ_0 divided by the volume of the unit cell a^2 , i.e., $B = \frac{\Phi_0}{a^2} \frac{p}{q}$, where $p, q \in \mathbb{N}$ are coprime, the phase factor becomes periodic with a period of q in y -direction. We can, hence, define a translational invariant lattice of magnetic unit cells with q lattice sites in y -direction. The non-interacting part of the Hamiltonian can now be transformed to momentum space yielding the $q \times q$ dispersion (or Harper) matrix of the system[1, 2]:

$$\varepsilon_{ll'}(\mathbf{k}) = \begin{pmatrix} -2t \cos(k_x) & -t & 0 & \dots & -te^{iqk_y} \\ -t & -2t \cos\left(k_x + \frac{2\pi p}{q}\right) & -t & 0 & \dots \\ & & \ddots & & \\ -te^{-iqk_y} & 0 & \dots & -t & -2t \cos\left(k_x + \frac{2\pi p(q-1)}{q}\right) \end{pmatrix},$$

Here we have set the lattice constant $a=1$. The Green's function $G(i\nu, \mathbf{k}) = [(i\nu + \mu)\mathbb{1}_{q \times q} - \varepsilon(\mathbf{k}) - \Sigma(i\nu, \mathbf{k})]^{-1}$ and the self-energy $\Sigma(i\nu, \mathbf{k})$ of the system are $q \times q$ matrices where the matrix indices correspond to the position of the lattice site within the magnetic unit cell. Within

the DMFT approximation a purely local self-energy is assumed which implies that the matrix $\Sigma(i\nu, \mathbf{k})$ does not depend on the momentum \mathbf{k} , has no off-diagonal elements (which would correspond to a nonlocal self-energy between different sites within the magnetic unit cell), and

is the same at all lattice sites due to the homogeneity of the system[1–4]. Hence, the self-energy matrix is proportional to a local scalar self-energy $\Sigma_{\text{loc}}(i\nu)$ times the $q \times q$ unit matrix. Within this approximation the corresponding DMFT lattice Green's function reads

$$G_{\text{DMFT}}(i\nu, \mathbf{k}) = \frac{1}{[i\nu + \mu - \Sigma_{\text{loc}}(i\nu)]\mathbb{1}_{q \times q} - \varepsilon(\mathbf{k})}. \quad (\text{S.4})$$

$\Sigma_{\text{loc}}(i\nu)$ can be obtained from an auxiliary Anderson impurity model (AIM):

$$\hat{H}_{\text{AIM}} = \underbrace{\sum_{n\sigma} \epsilon_n \hat{a}_{n\sigma}^\dagger \hat{a}_{n\sigma}}_{\hat{H}_{\text{bath}}} + \underbrace{\sum_{n\sigma} V_n \hat{a}_{n\sigma}^\dagger \hat{c}_\sigma + \hat{c}_\sigma^\dagger \hat{a}_{n\sigma}}_{\hat{H}_{\text{hyb}}} + \underbrace{U \hat{n}_\uparrow \hat{n}_\downarrow}_{\hat{H}_{\text{imp}}}, \quad (\text{S.5})$$

where $\hat{a}_{n\sigma}^{(\dagger)}$ annihilates (creates) an electron with spin σ at the (non-interacting) bath site n , ϵ_n is the local onsite energy of this bath site, $\hat{c}_\sigma^{(\dagger)}$ is the annihilation (creation) operator for an electron at the (interacting) impurity, V_n corresponds to the hybridization between the impurity and the bath and U denotes the interaction energy between two particles at the impurity. Model (S.5) can be solved numerically exactly by exact diagonalization (ED) if a finite number N of bath sites is considered. The bath parameters ϵ_n and V_n are determined by the condition that the impurity Green's function is equivalent to the local part of the DMFT Green's function in Eq. (S.4). This assumption is formally expressed by the selfconsistency condition

$$G_{\text{imp}}(i\nu) = \sum_{\mathbf{k}} [G_{\text{DMFT}}(i\nu, \mathbf{k})]_{ll}, \quad (\text{S.6})$$

where $\sum_{\mathbf{k}}$ denotes the normalized integral over the magnetic Brillouin zone defined by $k_x \in [-\pi, \pi)$ and $k_y \in [-\frac{\pi}{q}, \frac{\pi}{q})$. Note that all diagonal elements of the momentum-summed DMFT Green's function are equivalent due to the homogeneity of the problem.

B. Calculation of free energy

Within DMFT the lattice free energy F can be obtained from the impurity free energy F_{imp} via the following equation[5]

$$F = F_{\text{imp}} - \frac{1}{q} \frac{2}{\beta} \sum_{\nu \mathbf{k}} \ln \left(\det \left[\frac{G_{\text{imp}}(i\nu) \mathbb{1}_{q \times q}}{G_{\text{DMFT}}(i\nu, \mathbf{k})} \right] \right), \quad (\text{S.7})$$

where a factor of two in front of the frequency and momentum sum originates from the two spin projections of an electron. The impurity free energy F_{imp} is given by the difference between the free energy F_{AIM} of the AIM in Eq. (S.5) and the free energy F_{bath} of the bath, i.e., $F_{\text{imp}} = F_{\text{AIM}} - F_{\text{bath}}$, where $F_{\text{AIM}} = -\frac{1}{\beta} \ln Z_{\text{AIM}}$ and $F_{\text{bath}} = -\frac{1}{\beta} \ln Z_{\text{bath}}$. Within ED the partition functions Z_{AIM} and Z_{bath} of the entire AIM and the bath, respectively, can be straightforwardly evaluated as $Z_{\text{AIM}} = \text{Tr} e^{-\beta \hat{H}_{\text{AIM}}} = \sum_{j=1}^{4^{N+1}} e^{-\beta E_j}$ and $Z_{\text{bath}} = \text{Tr} e^{-\beta \hat{H}_{\text{bath}}} = \prod_{n=1}^N (1 + e^{-\beta \epsilon_n})^2$, where E_j denotes the numerically calculated eigenvalues of \hat{H}_{AIM} . Let us mention that within QMC the determination of F_{imp} is more difficult as a Wang-Landau algorithm[6] would be required to directly measure the partition function Z_{imp} of the impurity.

C. Numerical improvements

In our study we have performed calculations for various values of $B \sim \frac{U}{q}$ on a fine grid in the interval $[0, 0.5]$. This, however, requires rather large values of q corresponding to large sizes of the $q \times q$ matrix

$$M(i\nu, \mathbf{k}) = [i\nu + \mu - \Sigma_{\text{loc}}(i\nu)]\mathbb{1}_{q \times q} - \varepsilon(\mathbf{k}) \quad (\text{S.8})$$

in the denominator of Eq. (S.4). The calculation of the DMFT lattice Green's function $G_{\text{DMFT}}(i\nu, \mathbf{k})$ in Eq. (S.4) requires an inversion of this potentially large matrix while for the evaluation of the lattice free energy F in Eq. (S.7) the determinant of this matrix has to be calculated. These matrix operations typically scale as q^3 with the matrix size q and have to be carried out for all values of the fermionic Matsubara frequency ν and the momentum \mathbf{k} . Hence, this task can indeed become challenging for matrix sizes of the order of $q \sim 1000$. In the following, we will outline two numerical improvements based on (i) the specific structure of the matrix $M(i\nu, \mathbf{k})$ and (ii) a method which allows to find the fraction with the smallest denominator in a given interval.

1. Sherman-Morrison-Woodbury identities

The specific structure of the dispersion Matrix $\varepsilon(\mathbf{k})$ allows for a decomposition of the matrix $M(i\nu, \mathbf{k})$ as

$$M(i\nu, \mathbf{k}) = \underbrace{\begin{pmatrix} C_1^{\nu k_x} - t & t & 0 & \cdots & 0 \\ t & C_2^{\nu k_x} & t & \ddots & \vdots \\ 0 & \ddots & \ddots & \ddots & 0 \\ \vdots & \ddots & t & C_{q-1}^{\nu k_x} & t \\ 0 & \cdots & 0 & t & C_q^{\nu k_x} - t \end{pmatrix}}_{M_t(i\nu, k_x)} + t \underbrace{\begin{pmatrix} 1 \\ 0 \\ \vdots \\ 0 \\ e^{-iqk_y} \end{pmatrix}}_{M_{r1}(k_y) = \mathbf{v}(k_y) \otimes \mathbf{v}^\dagger(k_y)} \otimes (1 \ 0 \ \cdots \ 0 \ e^{iqk_y})$$

where we have used the short cut $C_j^{\nu k_x} = i\nu + \mu - \Sigma_{\text{loc}}(i\nu) + 2t \cos[k_x + 2\pi \frac{p(j-1)}{q}]$. We can now see that $M_t(i\nu, k_x)$ is a tridiagonal matrix depending on ν and k_x while $M_{r1}(k_y)$ depends only on k_y and is a matrix of rank one as it is built from the outer product of a complex vector $\mathbf{v}(k_y)$ and its complex conjugate. According to the Sherman–Morrison–Woodbury identities[7–9] we can now calculate the inverse and the determinant of the full (complex) matrix $M(i\nu, \mathbf{k})$ by evaluating the corresponding inverse and determinant of the (real) tridiagonal matrix $M_t(i\nu, k_x)$ plus (times) a specific correction term:

$$M^{-1} = M_t^{-1} - t \frac{M_t^{-1} \mathbf{v} \mathbf{v}^\dagger M_t^{-1}}{1 + \mathbf{v}^\dagger M_t^{-1} \mathbf{v}}, \quad (\text{S.9a})$$

$$\det M = \det M_t (1 + t \mathbf{v}^\dagger M_t^{-1} \mathbf{v}). \quad (\text{S.9b})$$

For better readability we have suppressed the dependencies of the matrices M and M_t as well as of the vector \mathbf{v} on ν , k_x and k_y . Eqs. (S.9) speed up our numerical calculations in two ways: (i) the evaluation of the inverse or the determinant of a tridiagonal matrix scales linearly with the matrix size q (in contrast to the cubic scaling q^3 for the full matrix); (ii) the actual calculation of the inverse or the determinant has to be performed independently only for all values of ν and k_x but not for k_y since the tridiagonal matrix M_t does not depend on k_y . Let us also note that due to the sparse structure of the vector \mathbf{v} (only two elements are non-zero) the numerical complexity of the matrix-vector multiplication $M_t^{-1} \mathbf{v}$ is independent of the matrix size q .

2. Minimal denominator in a given interval

To perform a comprehensive analysis of the free energy, double occupancy and quasiparticle lifetime as a function of the magnetic field we have used a very fine grid of roughly $N \sim 1500$ magnetic field points in the interval $B = \frac{p}{q} \in [0, 0.5]$. This corresponds to a set of magnetic fields $B = \frac{i}{2N}$, $i = 1, \dots, N$. Hence, we would have to perform N calculations with matrix size of $q = 2N$ which represents a considerable numerical effort in spite of the simplifications due to the specific structure of the dispersion matrix discussed in Sec. S1 C 1. We, hence, did not

conduct our calculations for magnetic fields corresponding to the edges of each interval $[\frac{i-1}{2N}, \frac{i}{2N}]$, $i = 1, \dots, N$ but rather for the fraction $\frac{p}{q} \in [\frac{i-1}{2N}, \frac{i}{2N}]$ with the *smallest* denominator in this interval. This fraction $\frac{p}{q} \in [\frac{i-1}{2N}, \frac{i}{2N}]$ can be determined by constructing a so-called Farey sequence[10] of intervals:

$$\left[\frac{a_{n+1}}{b_{n+1}}, \frac{c_{n+1}}{d_{n+1}} \right] = \begin{cases} \left[\frac{a_n + c_n}{b_n + d_n}, \frac{c_n}{d_n} \right], & \text{if } \frac{a_n + c_n}{b_n + d_n} < \frac{i-1}{2N} \\ \left[\frac{a_n}{b_n}, \frac{a_n + c_n}{b_n + d_n} \right], & \text{if } \frac{a_n + c_n}{b_n + d_n} > \frac{i}{2N}, \end{cases} \quad (\text{S.10})$$

where the starting values for our sequence are $a_0 = 0$ and $b_0 = c_0 = d_0 = 1$. We terminate the sequence at step n when either the fraction $\frac{a_n}{b_n}$ or the fraction $\frac{c_n}{d_n}$ is inside the interval $[\frac{i-1}{2N}, \frac{i}{2N}]$. This resulting fraction has then the smallest possible denominator in the given interval.

3. Improved frequency sums

Equation (S.7) for the evaluation of the DMFT lattice free energy F requires to sum the logarithm of the determinant of the impurity and DMFT lattice Green's function over all Matsubara frequencies. In practice, this sum has obviously to be truncated at a given finite frequency which gives rise to a truncation error. To mitigate this error we have expanded the addend in Eq. (S.7) in terms of $\frac{1}{i\nu}$:

$$\frac{1}{q} \sum_{\mathbf{k}} \ln \left(\det \left[\frac{G_{\text{imp}}(i\nu) \mathbb{1}_{q \times q}}{G_{\text{DMFT}}(i\nu, \mathbf{k})} \right] \right) = \frac{\sum_n V_n^2}{(i\nu)^2} + \mathcal{O} \left[\frac{1}{(i\nu)^3} \right]. \quad (\text{S.11})$$

We can subtract the first term on the right-hand side of this equation in the truncated numerical frequency sum and sum it up analytically for all frequencies which yields $-\frac{\beta}{4} \sum_n V_n^2$. This procedure improves considerably the accuracy of our numerical results as our truncation error depends cubically (instead of linearly) on the inverse cutoff frequency.

S2. INSULATOR-TO-METAL TRANSITION

In the main text we have demonstrated the emergence of a metal-to-insulator transition driven by a decrease of

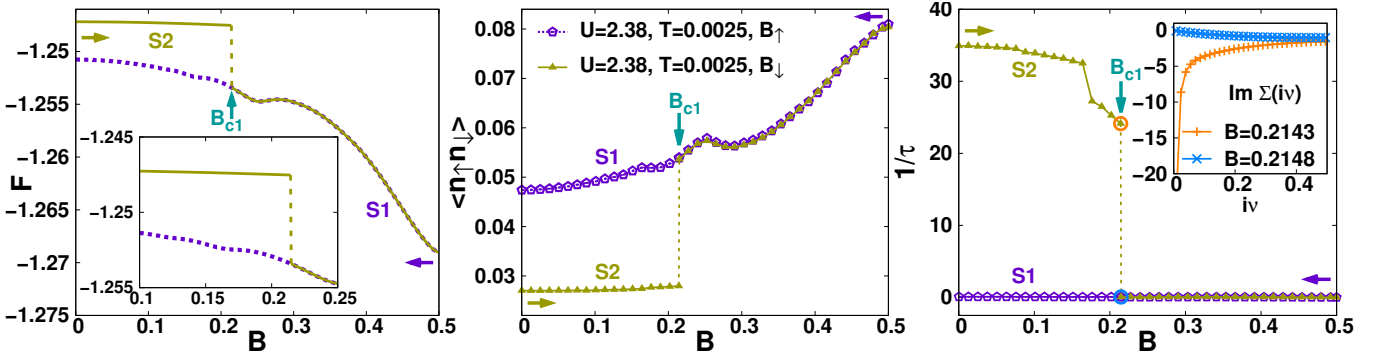


FIG. S1. Same as in Fig. 2 of the main text but for the point P2 in the phase diagram of Fig. 1 of the main text corresponding to the parameters $U = 2.38$ and $T = 0.0025$.

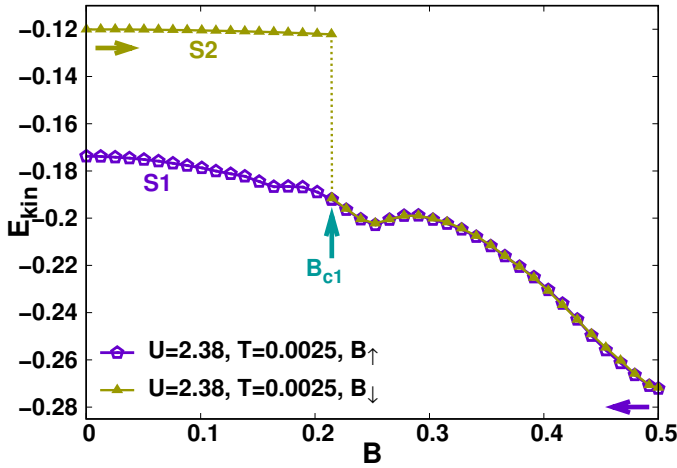


FIG. S2. Kinetic Energy for $U = 2.38$ and $T = 0.0025$ (corresponding to the point P2 in the phase diagram in Fig. 1 of the main text) as a function of the orbital magnetic field B obtained by the two sets of calculations B_{\uparrow} and B_{\downarrow} .

the orbital magnetic field (c.f. state S2 in Fig. 2 and the related discussion above). However, the expected opposite transition from an insulator to a metal triggered by an increase of the orbital magnetic field could not be observed since the corresponding boundary B_{c1} between the coexistence region and the pure metallic state has not been reached for the largest magnetic field $B = 0.5$. To verify the possibility of an insulator-to-metal transition driven by an orbital magnetic field we have, hence, to consider other values of U and/or T . To this end we have selected the point P2 in Fig. 1 of the main text which is located inside the metallic part of the coexistence regime (for the system without magnetic field) and characterized by the interaction parameter $U = 2.38$ and the temperature $T = 0.0025$. At this point in the phase diagram, we can, hence, stabilize the insulating phase for $B = 0$ which we label S2 (solid olive line in the left panel of Fig. S1). Upon increasing B , we indeed find a transition from this insulating state S2 to a metallic phase at a magnetic field $B_{c1} = 0.2143$ where the state S2 collapses onto S1. On

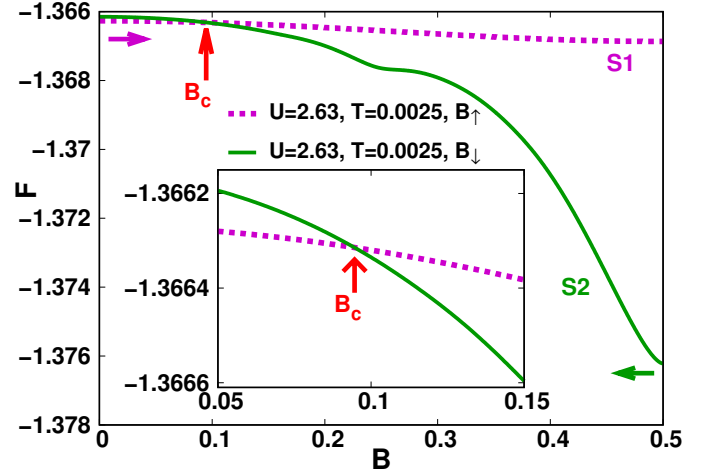


FIG. S3. Same as left panel in Fig. 2 of the main text but for the point P4 in the phase diagram of Fig. 1 of the main text corresponding to the parameters $U = 2.63$ and $T = 0.0025$.

the contrary, for the complementary set of calculations where we start at $B = 0.5$ and decrease the magnetic field (B_{\downarrow} , dashed violet line) the system remains in the metallic state at all values of the magnetic field. This proves that B_{c1} indeed marks the boundary between the coexistence and the metallic regime as a function of the orbital magnetic field B , i.e., for $B > B_{c1}$ the system is in the pure metallic phase.

To confirm the nature of the two states S1 and S2 we have calculated the double occupancy $D = \langle n_{\uparrow}n_{\downarrow} \rangle$ for both solutions (middle panel of Fig. S1). We find a very low value for the state S2 (olive triangles) for $B < B_{c1}$ indicative of a Mott insulator where almost each lattice site is occupied by only one electron. On the contrary the double occupancy for S1 (violet pentagons) is much larger corresponding to a metallic behavior of the system. This is also true for S2 at $B > B_{c1}$ where this state becomes equivalent to S1.

A corresponding behavior is found for the inverse quasiparticle lifetime and the electronic self-energy in the right panel of Fig. S1. For the solution S2 (olive triangles)

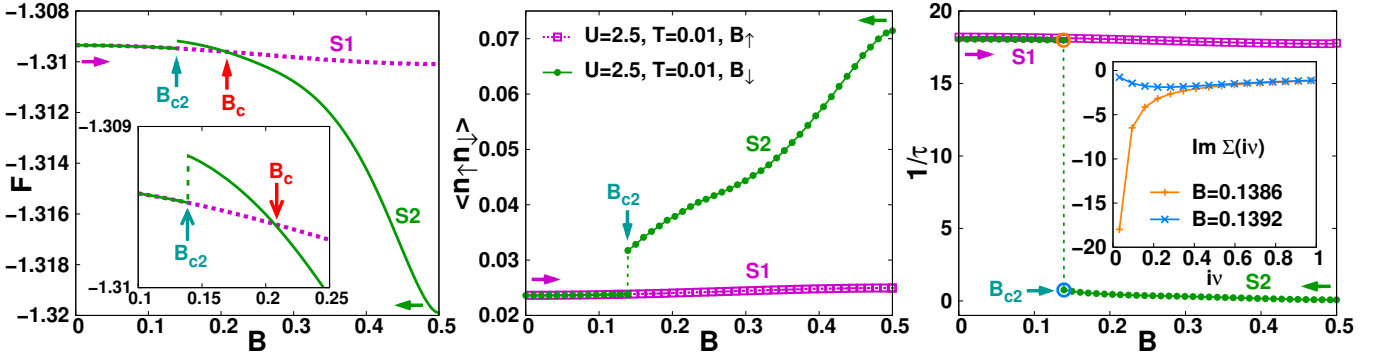


FIG. S4. Same as in Fig. 2 of the main text but for point P4 in the phase diagram of Fig. 1 of the main text corresponding to the parameters $U=2.5$ and $T=0.01$.

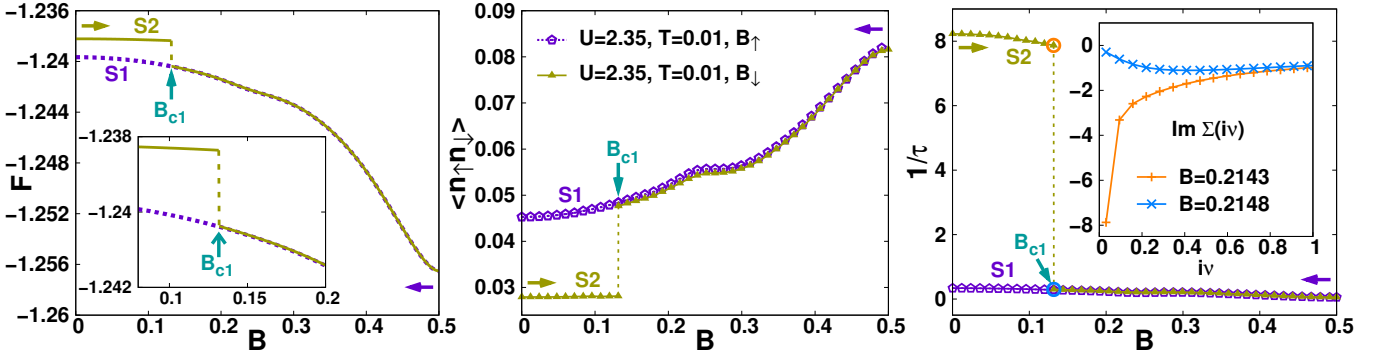


FIG. S5. Same as in Fig. 2 of the main text but for point P5 in the phase diagram of Fig. 1 of the main text corresponding to the parameters $U=2.35$ and $T=0.01$.

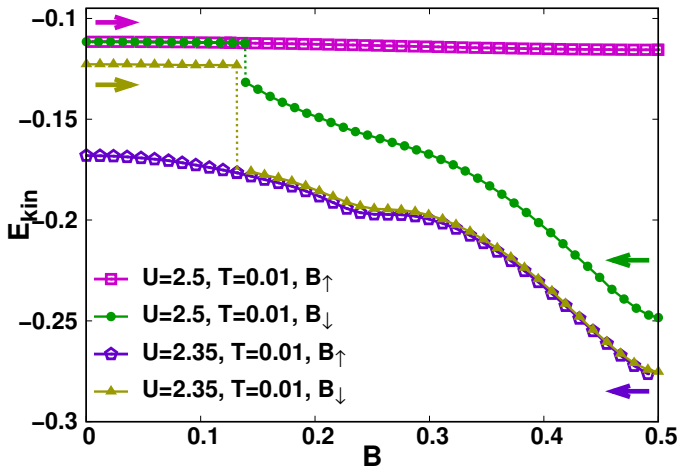


FIG. S6. Kinetic Energy for $U=2.34$ and $U=2.5$ at $T=0.01$ (corresponding to points P4 and P5, respectively, in the phase diagram in Fig. 1 of the main text) as a function of the orbital magnetic field B obtained by the two sets of calculations B_{\uparrow} and B_{\downarrow} discussed in Fig. S5.

$1/\tau$ is very large for $B < B_{c1}$ which is typically observed in a Mott insulator. For larger values of $B > B_{c1}$ it drops by several orders of magnitude and becomes equivalent

to the solution S1 (violet pentagons) which is metallic in the entire B region. The inset depicts the corresponding qualitative difference in the electronic self-energy on the left- and right-hand side of B_{c1} . It is non-monotonous in the metallic phase showing an upturn at low frequencies for $B \gtrsim B_{c1}$ (blue crosses) while it diverges in the insulating state at $B \lesssim B_{c1}$ (orange pluses).

We complete our analysis of P2 by discussing the kinetic energy of the system as a function of the magnetic field strength. As for P1 in the main text, the kinetic energy is very small (in absolute value) and weakly B dependent in the insulating state S2 for $B < B_{c1}$ (olive triangles in Fig. S2). For the metallic solution S1 (violet pentagons) on the other hand, to which S2 collapses for $B > B_{c1}$, the kinetic energy is much larger and features a substantial variation with the magnetic field strength.

Let us finally remark that for the point P2 in the phase diagram of Fig. 1 the free energy of the metallic solution is *always* lower than the one of the insulator (see left panel of Fig. S1). Hence, for this set of parameters only a coexistence between the two phases but no real phase transition in the thermodynamics sense is observed.

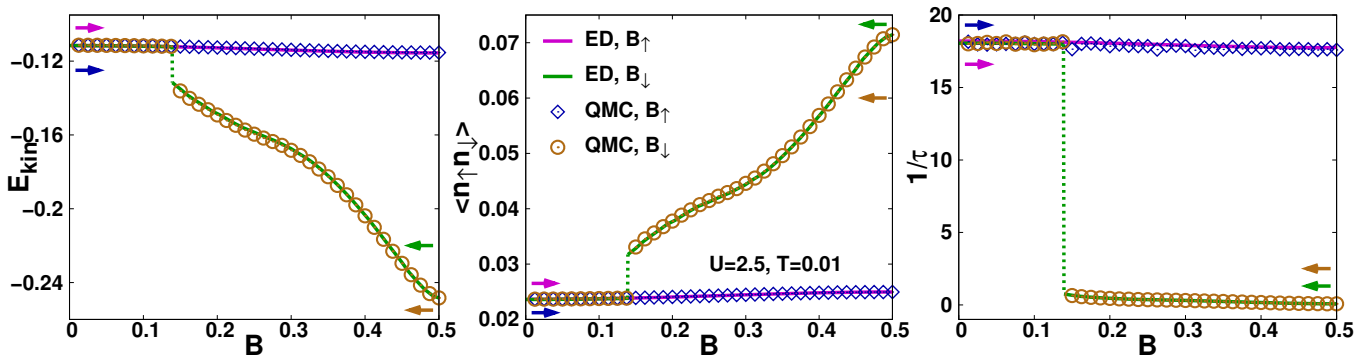


FIG. S7. Kinetic energy E_{kin} (left panel), double occupancy $D = \langle n_{\uparrow} n_{\downarrow} \rangle$ (middle panel) and inverse quasi-particle lifetime $1/\tau = -\text{Im}\Sigma(i\nu_1)$, $\nu_1 = \frac{\pi}{\beta}$ (right panel), for $U=2.5$ and $T=0.01$ as a function of the orbital magnetic field B obtained from ED and QMC calculations. B_{\uparrow} and B_{\downarrow} indicate that the calculations have been started at $B=0$ and $B=0.5$, respectively.

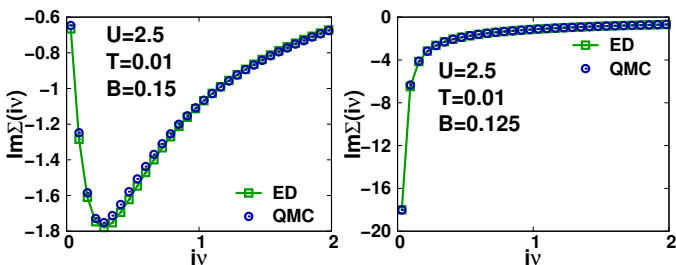


FIG. S8. ED vs. QMC self-energies for $U=2.5$ and $T=0.01$ for two magnetic fields slightly above (left panel) and below (right panel) the phase transition between the insulating and the metallic phase in Fig. S4.

S3. ADDITIONAL DATA

In this section, we present results for the points P3, P4 and P5 in the phase diagram of Fig. 1 of the main text corresponding to $U=2.63$ and $T=0.025$ as well as $T=0.01$ for $U=2.5$ and $U=2.34$, respectively. In Fig. S3 we depict the free energy at point P3 which corresponds to a slightly smaller value of $U=2.63$ than the one discussed in Fig. 2 in the main text ($U=2.68$). Since the system is more metallic in this case, the critical magnetic field $B_c = 0.0946$, where the free energy of the insulator becomes lower than the one of the metal, is smaller for $U=2.63$ with respect to $U=2.68$ (where we find $B_c = 0.2077$). Moreover, P3 is located in the (insulating part of the) coexistence region of the field-free model and, hence, the metallic solution can be stabilized down to $B=0$. This implies that the system is in the coexistence region for all values of B and, hence, the coexistence region boundaries B_{c1} and B_{c2} , which would be indicated by a discontinuity in the free energy, cannot be observed in this case.

Let us finally address the results for the points P4 and P5 in the phase diagram 1 of the main text which correspond to the higher temperature $T=0.01$. As for the points P1 and P2 we present the free energy, double occupancy and inverse quasi-particle life times in Figs. S4 and

S5 for $U=2.5$ (P4) and $U=2.34$ (P5), respectively. The kinetic energies are depicted for both parameter sets in Fig. S6. The results for P4 and P5 are completely analogous to the ones for P1 and P2 and, hence, we refer the reader to the discussion of the latter for a detailed description.

S4. COMPARISON WITH QMC CALCULATIONS

In this section, we present benchmarks of our ED calculations against corresponding QMC results obtained from a continuous time quantum Monte Carlo solver in its hybridization expansion implementation as provided by the `w2dynamics` package[11]. We focus on the point P4 in the phase diagram of Fig. 1 in the main text corresponding to the parameters $U=2.5$ and $T=0.01$. We find an excellent agreement between QMC and ED data for the kinetic energy E_{kin} , the double occupancy D and the inverse quasi-particle lifetime $1/\tau$, in the left, middle and right panel of Fig. S7, respectively. In particular, the magnetic field B_{c2} defining the boundary between the coexistence region and the insulating state is the same for ED and QMC which confirms the robustness of our ED calculations. Let us mention, that the fluctuations in the QMC results for the inverse quasi-particle life time $1/\tau$ in the insulating solution (orange circles for $B < B_{c2}$ and blue diamonds) originate from statistical noise which can be systematically improved by increasing the number of Monte Carlo samples in the simulation.

Finally, in Fig. S8 we show a comparison between ED (green empty squares) and QMC (blue empty circles) self-energies for point P4 in the phase diagram Fig. 1 in the main text. The magnetic fields correspond to the metallic regime right above B_{c2} (left panel) and the insulating regime right below B_{c2} (right panel) in Fig. S4, respectively. The agreement between ED and QMC is indeed excellent for the insulating case while for the metallic state small deviations at small frequencies can be observed. This tiny discrepancy originates from the fact the

in the metallic part of the phase diagram a finite number of bath sites cannot exactly provide the Kondo screening of the local moment. However, such small deviations

in $\Sigma(i\nu)$ do not play a role for the observed phase transition and the related thermodynamic quantities as we have seen in Fig. S7.

-
- [1] A. A. Markov, G. Rohringer, and A. N. Rubtsov, *Phys. Rev. B* **100**, 115102 (2019).
 - [2] J. Vučičević and R. Žitko, *Phys. Rev. B* **104**, 205101 (2021).
 - [3] S. Acheche, L.-F. Arsenault, and A.-M. S. Tremblay, *Phys. Rev. B* **96**, 235135 (2017).
 - [4] J. c. v. Vučičević and R. Žitko, *Phys. Rev. Lett.* **127**, 196601 (2021).
 - [5] A. Georges, G. Kotliar, W. Krauth, and M. J. Rozenberg, *Rev. Mod. Phys.* **68**, 13 (1996).
 - [6] F. Wang and D. P. Landau, *Phys. Rev. Lett.* **86**, 2050 (2001).
 - [7] J. Sherman and W. J. Morrison, *The Annals of Mathematical Statistics* **21**, 124 (1950).
 - [8] W. W. Hager, *SIAM Review* **31**, 221 (1989), <https://doi.org/10.1137/1031049>.
 - [9] D. A. Harville, *Matrix Algebra From a Statistician's Perspective* (Springer-Verlag, New York, 1997).
 - [10] I. M. Niven, H. S. Zuckerman, and H. L. Montgomery, *An Introduction to the Theory of Numbers*, 5th ed. (John Wiley and Sons, New York, 1991).
 - [11] M. Wallerberger, A. Hausoel, P. Gunacker, A. Kowalski, N. Parragh, F. Goth, K. Held, and G. Sangiovanni, *Computer Physics Communications* **235**, 388 (2019).